

## SITE PREFERENCES OF HYPERFINE IMPURITIES IN $\text{Ni}_2\text{Al}_3$ PHASES

Matthew O. Zacate and Gary S. Collins

*Department of Physics, Washington State University, Pullman, WA 99164, USA*

The site occupation of indium solutes in  $\text{Ni}_2\text{Al}_3$ -type compounds was determined using perturbed angular correlation of gamma rays. Measurements were made for compositions on both sides of the stoichiometric composition. Sites were identified through their quadrupole interactions. For transition-metal (TM) rich aluminides and galliumides, indium solutes occupy only one of two inequivalent trivalent-metal sites (Al or Ga). For TM-poor aluminides, indium solutes tend to locate at non-crystallographic sites such as in grain boundaries. For TM-poor galliumides, the solutes occupy nickel sites while close to the stoichiometric composition they also occupy sites on an empty Ni-sublattice. Composition dependences of site preference for indium solutes in  $\text{Pt}_2\text{Al}_3$  and  $\text{Ni}_2\text{Ga}_3$  are examined in terms of a recently developed thermodynamic model.

Locations of solutes in binary compounds are of general interest because they affect material properties. In this paper we report in detail on measurements of site preference of dilute indium solutes in two compounds having the  $\text{Ni}_2\text{Al}_3$  structure,  $\text{Ni}_2\text{Ga}_3$  and  $\text{Pt}_2\text{Al}_3$ . We also summarize results of measurements in  $\text{Ni}_2\text{Al}_3$ ,  $\text{Pd}_2\text{Al}_3$  and  $\text{Pt}_2\text{Ga}_3$  and in the indiumides  $\text{Ni}_2\text{In}_3$ , and  $\text{Pt}_2\text{In}_3$  in which indium is a host atom. A full account of measurements on these compounds will be given elsewhere [1]. The locations of  $^{111}\text{In}/\text{Cd}$  probes used as solutes are determined through the quadrupole interaction between probe nuclei and electric-field gradients (efgs) using perturbed angular correlation of gamma rays (PAC). The structure, shown in figure 1, can be derived from the CsCl structure by removal of every third 111-plane of Ni-atoms followed by a slight contraction ( $\sim 1\%$ ) along the 111 direction and shufflings of occupied planes toward the empty planes. As a result there are four inequivalent lattice sites in the perfect  $\text{A}_2\text{B}_3$  structure: site  $\alpha$  occupied by A-atoms, sites  $\beta 1$  and  $\beta 2$  occupied by B-atoms, and site X empty. The relative numbers of sites  $\alpha:\beta 1:\beta 2:X$  are 2:1:2:1.

Sites were identified through comparison of quadrupole interactions with those measured in the indiumides and through calculations of efgs. All sites have three-fold rotational axes of point symmetry and therefore axially-symmetric efgs. Large differences in the magnitudes of efgs of the four sites are expected. Neglecting the slight contraction and shufflings, the local structures around the  $\alpha$  and X sites are both cubic out to the third atomic shell. As a consequence, the efgs at those sites should be close to zero. On the other hand, the  $\beta 1$  and  $\beta 2$  sites both have non-cubic atomic arrangements in their first atomic shells, and therefore one expects large efgs. Explicit calculations of efgs were carried out in the point charge approximation using lattice parameters representative of those of the eight phases. For a ratio of effective charges  $Q(\alpha)/Q(X) = 0.2$ , the magnitudes of the principal components of the efgs at the four sites are in the proportions  $V_{zz}(\alpha):V_{zz}(\beta 1):V_{zz}(\beta 2):V_{zz}(X) = 0.1:1.6:1.0:0.1$ , reproducing the experimental ratio  $V_{zz}(\beta 1)/V_{zz}(\beta 2) \cong 1.6$  for the indiumides. These

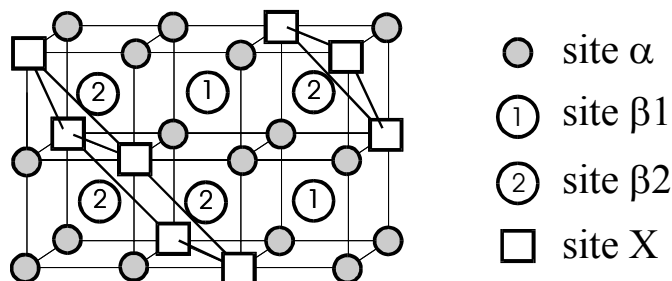


Figure 1.  $\text{Ni}_2\text{Al}_3$  structure referenced to the CsCl structure to which it is related (see text). Four inequivalent sites shown by a (shaded circle),  $\beta 1$  and  $\beta 2$  (numbered circles, and X (square).

calculations also confirm that efgs for sites  $\alpha$  and X are comparable in magnitude and much smaller than for  $\beta$ -sites.

Samples were prepared by arc-melting high purity metal foils on which carrier-free  $^{111}\text{In}$  has been deposited. The fractional concentration of  $^{111}\text{In}$  was less than  $10^{-8}$ . Samples were annealed to equilibrate the  $\text{Ni}_2\text{Al}_3$  phase and to coarsen the grain structure. Nominal sample compositions were determined from masses of the starting foils, and adjusted by less than or about 0.5 at.% to account for minor mass losses during arc-melting that were attributed to evaporation of the more volatile element. Further details will be given elsewhere [1]. Measurements were made at room temperature on eight  $\text{Ni}_2\text{Ga}_3$  and two  $\text{Pt}_2\text{Al}_3$  samples using a standard four-detector PAC spectrometer [2]. From computer fits of the spectra were obtained fractions of the solutes in the different sites, fundamental measured quadrupole interaction frequencies,  $\omega_1$ , proportional to  $V_{zz}$ , and efg asymmetry parameters,  $\eta$ . Spectra have been corrected for offsets due to source self-absorption [3].

PAC spectra for  $\text{Ni}_2\text{Ga}_3$  and  $\text{Pt}_2\text{Al}_3$  are shown in Fig. 2 for compositions on either side of the stoichiometric 40:60 composition. (While published phase diagrams show these phases as line compounds, they appear from our measurements to have field widths of order 1 at.% as shown below.) For comparison, spectra for stoichiometric  $\text{Ni}_2\text{In}_3$  and  $\text{Pt}_2\text{In}_3$  are also shown. Because indium is a host element in the two indiumides, it must occupy the  $\beta_1$ - and  $\beta_2$ -sites. As expected, two quadrupole interactions with site-fractions in a ratio of 1:2 were observed in each phase. The frequencies in  $\text{Ni}_2\text{In}_3$  are  $\omega_1(\beta_1) = 244.8(8)$  Mrad/s and  $\omega_1(\beta_2) = 145.8(3)$  Mrad/s and in  $\text{Pt}_2\text{In}_3$  are  $\omega_1(\beta_1) = 263.9(6)$  Mrad/s and  $\omega_1(\beta_2) = 169.1(3)$  Mrad/s, in good agreement with previous work [4]. In addition, the two indiumides each exhibited a defect-associated signal with small site-fraction that is not discussed further in this paper.

Immediately below spectra for the indiumides in Fig. 2 are shown spectra for  $\text{Ni}_2\text{Ga}_3$  and  $\text{Pt}_2\text{Al}_3$  on the TM-rich side of stoichiometry. Each exhibits only a single quadrupole interaction, with frequencies  $\omega_1 = 164.9(9)$  Mrad/s and  $\omega_1 = 180.1(3)$  Mrad/s, respectively. These frequencies are slightly larger than, but close to, frequencies  $\omega_1(\beta_2)$  in the corresponding indiumides. The indiumides have a larger unit-cell volume, and when the volume-dependence of the efg is taken into account (e.g.  $V_{zz} \propto (\text{volume})^{-1}$  in the point-charge approximation), the agreement with  $\omega_1(\beta_2)$  is excellent. Thus, indium solutes in TM-rich  $\text{Ni}_2\text{Ga}_3$  and  $\text{Pt}_2\text{Al}_3$  strongly prefer site  $\beta_2$ . The same conclusion was reached for the other two aluminides and galliumide. An axially-symmetric signal with  $\omega_1 \cong 278$  Mrad/s that may correspond to probes at the  $\beta_1$  site was observed at the 2% level in  $\text{Ni}_2\text{Ga}_3$ , but the  $\beta_2$ -site is by far the favored location, as in  $\text{Pt}_2\text{Al}_3$  and the other three TM-rich compounds. The atomic volume of site  $\beta_2$  can be shown to be 10% larger than of site  $\beta_1$ , providing a possible explanation why an oversized solute such as indium prefers site  $\beta_2$ .

Spectra of  $\text{Ni}_2\text{Ga}_3$  samples at the stoichiometric composition (39.9 at.% Ni) and at 37.4 at.% Ni are also shown in Fig. 2. Both spectra exhibit small  $\beta_2$  site fractions. The spectrum for the 37.4 at.% sample is dominated by a zero-frequency signal in place of the  $\beta_2$  signal. The spectrum for the stoichiometric sample exhibits both the zero-frequency signal and a low-frequency signal with  $\omega_1 = 15(4)$  Mrad/s and  $\eta \sim 0$ . These zero- and low frequency signals were found not to be associated with neighboring phases and therefore are attributed to  $\alpha$  and X sites of the  $\text{Ni}_2\text{Ga}_3$  phase, but a further assignment cannot be made on the basis of hyperfine parameters alone. It will be shown below from thermodynamic modeling of the composition

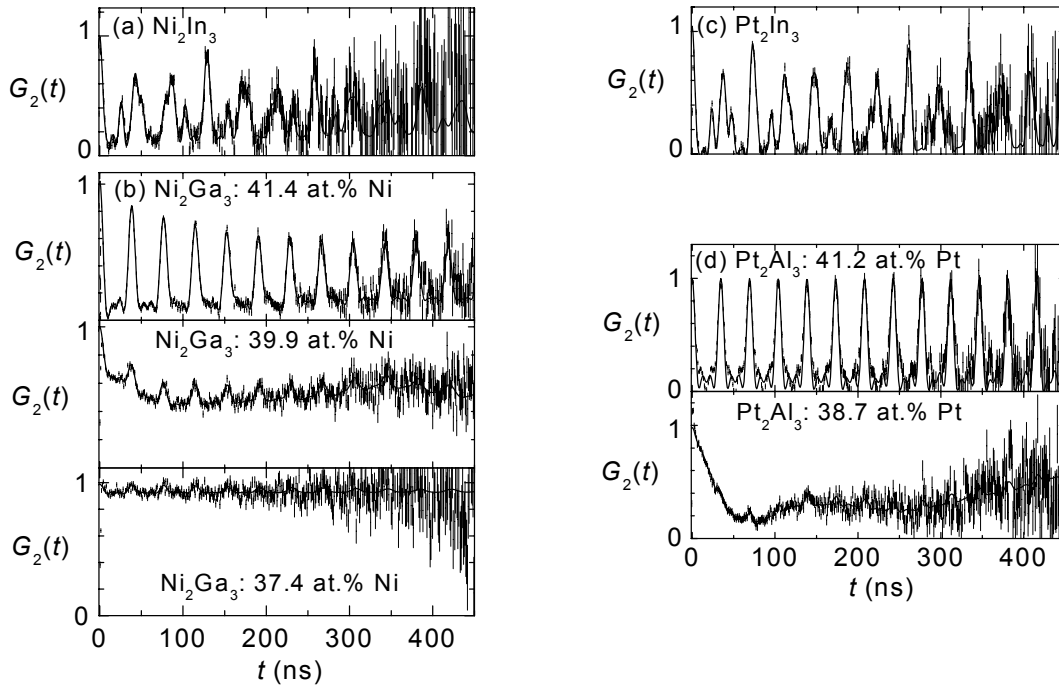


Figure 2. PAC spectra from (a)  $\text{Ni}_2\text{In}_3$ , (b) the Ni-Ga system near the  $\text{Ni}_2\text{Ga}_3$  stoichiometric composition, (c)  $\text{Pt}_2\text{In}_3$ , and (d) the Pt-Al system near the  $\text{Pt}_2\text{Al}_3$  stoichiometric composition..

dependence of site fractions that the zero-frequency signal corresponds to site  $\alpha$  and the low-frequency signal to site X. Similar behavior was observed in  $\text{Pt}_2\text{Ga}_3$  (not shown).

For Pt-poor  $\text{Pt}_2\text{Al}_3$  is observed a small  $\beta_2$  site-fraction ( $\sim 10\%$ ), a zero-frequency signal ( $\sim 25\%$ ), and a large site-fraction ( $\sim 65\%$ ) that has significant inhomogeneous broadening with  $\omega_1 = 35.5(4)$  Mrad/s and  $\eta = 0.47(3)$ . There is some uncertainty in the cubic fraction due to texturing and a large offset correction due to source self-absorption. Based on the very small broadening of the  $\beta_2$ -signal visible in the spectrum for 41.2 at.% Pt, the crystal structure is clearly highly ordered. Therefore, the inhomogeneous 35.5 Mrad/s signal cannot be attributed to regular lattice sites but instead to non-crystallographic sites such as in grain boundaries, interfaces or dislocations. By analogy with  $\text{Ni}_2\text{Ga}_3$ , the zero-frequency signal will be attributed to site  $\alpha$ . Similar behavior was observed in  $\text{Ni}_2\text{Al}_3$  and  $\text{Pd}_2\text{Al}_3$  (not shown).

Fitted site-fractions from  $\text{Ni}_2\text{Ga}_3$  are plotted in Fig. 3(a) as a function of  $x$ , which is the deviation from stoichiometry according to  $\text{Ni}_{2+5x}\text{Ga}_{3-5x}$ . It can be seen that indium predominantly occupies different sites on different sides of the stoichiometric composition, and site-fractions cross over rapidly near stoichiometry. The site-fraction of the low-frequency signal has a maximum near stoichiometry. This site-preference behavior can be reproduced using a recently developed thermodynamic model [5, 6]. In the model, ratios of site fractions are found to be proportional to fractional concentrations of intrinsic point defects. In the  $\text{A}_2\text{B}_3$  structure, defects of interest are vacancies and antisite atoms on the three substitutional sublattices  $\alpha$ ,  $\beta_1$  and  $\beta_2$ , and host atoms A and B in empty X-sublattice sites that have the character of interstitial sites. For simplicity, the energies of defects (but not solutes) on the  $\beta_1$  and  $\beta_2$  sublattices are assumed to be equal in the following analysis. Four ratios can be written as  $R_\alpha^{\beta_2} \equiv f_{\beta_2}/f_\alpha = [A_\beta] \exp(+G_{a_2}/k_B T)$ ,  $R_X^{\beta_2} = 2[A_\beta][V_\alpha] \exp(+G_{g_2}/k_B T)$ ,  $R_X^\alpha = 2[V_\alpha] \exp(+G_h/k_B T)$ , and  $R_{\beta_1}^{\beta_2} = 2 \exp(+G_k/k_B T)$ , in which fractional concentrations are in square brackets and in which the  $G$ 's are changes in free energy when a solute  $S$  is transferred

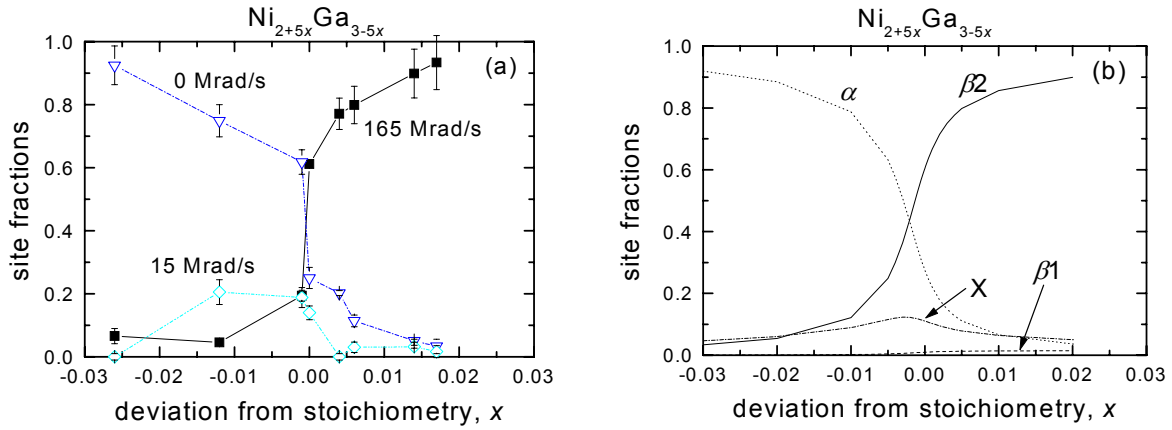


Figure 3. Site fractions in  $\text{Ni}_2\text{Ga}_3$  versus composition: (a) experimental; (b) thermodynamic model simulation.

between sublattices:  $G_{a_2} = G(S_\alpha) - G(S_{\beta_2}) + G(A_\beta)$ ,  $G_{g_2} = G(S_X) - G(S_{\beta_2}) + G(A_\beta) + G(V_\varepsilon)$ ,  $G_h = G(S_X) - G(S_\alpha) + G(V_\alpha)$ , and  $G_k = G(S_{\beta_1}) - G(S_{\beta_2})$ , wherein the  $G()$  are site-energies of the defects or solutes. The site-fractions are obtained trivially from the ratios via  $f_{\beta_2} = (1 + 1/R_{\beta_1}^{\beta_2} + 1/R_\alpha^{\beta_2} + 1/R_X^{\beta_2})^{-1}$ ,  $f_{\beta_1} = (1 + R_{\beta_1}^{\beta_2} + R_{\beta_1}^{\beta_2}/R_\alpha^{\beta_2} + R_{\beta_1}^{\beta_2}/R_X^{\beta_2})^{-1}$ ,  $f_\alpha = (1 + R_\alpha^{\beta_2} + R_\alpha^{\beta_2}/R_{\beta_1}^{\beta_2} + 1/R_X^\alpha)^{-1}$ , and  $f_X = (1 + R_X^\alpha + R_X^{\beta_2} + R_X^{\beta_2}/R_{\beta_1}^{\beta_2})^{-1}$ . Whether or not a solute switches sites as the composition changes from one side of stoichiometry to the other depends on the relative magnitudes of solute-transfer energies and defect energies, as discussed in refs. [5] and [6].

An explicit simulation was made of site-fractions in  $\text{Ni}_2\text{Ga}_3$  using the model, with results shown by the curves in Fig. 3(b). Parameters used were 6.41, 6.91, -0.14, 0.90, -5.64, -5.32, 0.96, 0.60, 0.40, and -5.14 eV for  $G(V_\alpha)$ ,  $G(V_\beta)$ ,  $G(A_\beta)$ ,  $G(B_\alpha)$ ,  $G(A_X)$ ,  $G(B_X)$ ,  $G(S_\alpha)$ ,  $G(S_{\beta_1})$ ,  $G(S_{\beta_2})$ , and  $G(S_X)$ , respectively. In addition, the cohesive enthalpy of the unit cell was taken to be -29.02 eV, and the simulation temperature was 450 °C. As can be seen, it is possible to reproduce both the crossover behavior and maximum near stoichiometry. Such a maximum can only be simulated for an empty-lattice or interstitial site [5,6]. Therefore, the low-frequency signal is attributed to site X and, by default, the zero-frequency signal must be attributed to site  $\alpha$ . It should be recognized that the set of parameters used in the simulation is not unique and that other sets lead to the same qualitative behavior.

In summary, this study has experimentally revealed the site-preference of a solute (1) for one of two inequivalent sites of an element, (2) between sites of different elements, (3) between substitutional and empty-lattice (interstitial) sites, and (4) between substitutional and noncrystallographic sites such as in grain-boundaries.

The authors thank Bonner C. Walsh for assistance with experiments. This work was supported in part by National Science Foundation grants DMR 96-12306 and 00-91681.

1. Matthew O. Zacate and Gary S. Collins (to be published.)
2. G.S. Collins, S.L. Shropshire and J. Fan, *Hyp. Interact.* 62 (1990) 1.
3. A. R. Arends et al., *Hyp. Interact.* 8 (1980) 191.
4. R. Platzler et al., *Hyp. Interact.* 60 (1990) 1003; M. Marszalek et al., *Hyp. Interact.* 80 (1993) 1029.
5. Gary S. Collins and Matthew O. Zacate, *Hyp. Interact.* (this conference).
6. Gary S. Collins and Matthew O. Zacate, (to be published).